EUROPEAN ORGANIZATION FOR NUCLEAR RESEARCH

CERN-EP/84-33
19 March 1984

INCLUSIVE $K^{*o}(890)$ AND $\bar{K}^{*o}(890)$ PRODUCTION ON BERYLLIUM BY K^- and π^- AT 175 GeV

ACCMOR Collaboration
Amsterdam[1]-Bristol[2]-CERN[3]-Cracow[4]-Munich[5]-Rutherford[6] Collaboration

R. Bailey[6], D.G. Bardsley[2], E. Belau[5], T. Böhringer[3], M. Bosman[3], M. Cerrada[3], V. Chabaud[3], C. Damerell[6], C. Daum[1], G. De Rijk[1], H. Dijkstra[1], A. Dwurazny[4], A. Gillman[6], R. Gilmore[2], L. Görlich[5], Z. Hajduk[4], C. Hardwick[1], W. Hoogland[1], B.D. Hyams[3], R. Klanner[5], G. Lutz[5], J. Malos[2], W. Männer[5], G. Polok[4], G. Lütjens[5], M. Rozanska[4], K. Rybicki[4], H.J. Seebrunner[5], W. Spierenburg[1], U. Stierlin[5], R.J. Tapper[2], H.G. Tiecke[1], M. Turala[4], J. Vermeulen[3], G. Waltermann[5], P. Weilhammer[3], F. Wickens[6], L.W. Wiggers[1], A. Wylie[5] and T. Zeludziewicz[5*)]

ABSTRACT

The reactions $K^-Be \to (\bar{K})^{*o}(890)X$, $\pi^-Be \to (\bar{K})^{*o}(890)X$ have been studied in a 175 GeV unseparated hadron beam in the kinematic range $0 < x_F < 1.0$ and $p_T^2 < 5$ GeV^2. Integrated cross-sections and the dependence of the cross-sections on the longitudinal and transverse momentum are presented, together with quark counting rules predictions. The nuclear dependence of K^- fragmentation into $\bar{K}^{*o}(890)$ with respect to Feynman x is investigated from hydrogen to beryllium.

Submitted to Zeitschrift für Physik C

---

1) NIKHEF-H, Amsterdam, The Netherlands
2) University of Bristol, Bristol, UK
3) CERN, Geneva, Switzerland
4) Institute of Nuclear Physics, Cracow, Poland
5) Max Planck Institut für Physik, Munich, Fed. Rep. Germany
6) Rutherford Laboratory, Chilton, Didcot, UK
*) Visitor from Institute of Nuclear Physics, Cracow, Poland

1. INTRODUCTION

During the last few years, studies of low-p_T hadronic collisions have changed their focus of interest from single-particle inclusive production to multiparticle inclusive production, in particular resonance inclusive production. Single-particle studies suffer from the fact that it is hard to distinguish between direct production of these particles and intermediate production through the decay of resonances or particles such as the K^*, ρ, or Λ. Proposed particle-production mechanisms of the quark-recombination type, the quark-fragmentation type, or the perturbative QCD approach describe successfully a large number of single-particle inclusive processes (see reference [1] for a description of the different mechanisms). It is hoped that data on multiparticle production will succeed in discriminating between these different approaches. A recent review [2] summarizes both the theoretical and the experimental situations at the present time.

Several results have been published on $K^*(890)$ inclusive production by incoming pions, kaons, and protons on hydrogen in the energy range 12-110 GeV [3]. Owing to a lack of statistics for large Feynman x values and problems with particle identification, only leading-particle channels were studied (a leading particle channel is a channel in which the incident particle and the outgoing particle share a common valence quark).

In this paper we present results from a high-statistics study of $K^{*o}(890)$ and $\bar{K}^{*o}(890)$ production on beryllium at 175 GeV by incoming π^- and K^-. In the same experiment we study four different reactions:

a) $K^-Be \rightarrow \bar{K}^{*o}(890) + X$ $\quad$ $(\bar{u}s)$ $\quad$ $(\bar{d}s)$

b) $K^-Be \rightarrow K^{*o}(890) + X$ $\quad$ $(\bar{u}s)$ $\quad$ $(d\bar{s})$

c) $\pi^-Be \rightarrow \bar{K}^{*o}(890) + X$ $\quad$ $(\bar{u}d)$ $\quad$ $(\bar{d}s)$

d) $\pi^-Be \rightarrow K^{*o}(890) + X$ $\quad$ $(\bar{u}d)$ $\quad$ $(d\bar{s})$

Reactions (a) and (d) are examples of leading particle channels according to the above definition.

The paper is organized as follows. In Section 2 we give a short description of the apparatus and we present the amount of triggers collected from which the data were extracted. In Section 3 we describe the analysis method, and in Section 4 results on longitudinal (Feynman x) and transverse momentum (p_T^2) differential distributions, integrated cross-sections, and a result on the nuclear dependence of reaction (a).

2. THE EXPERIMENT

The data were taken at the CERN SPS with the NA11 forward spectrometer. A schematic layout of the experimental set-up is shown in fig. 1 and it is extensively described in ref.[4]. Here we only give a short description of the apparatus, concentrating on elements relevant to this experiment.

The beam particle is identified by two differential Cherenkov counters (CEDARs). The target consists of a set of four 2 mm high, 20 mm wide, and 8 mm long beryllium slabs, each followed by a thin scintillation counter. These thin counters locate the target cell in which the interaction took place, and are used to trigger the apparatus to accept events where three or more charged secondary particles are produced. A small scintillation counter D2, placed after the second dipole magnet, is used to veto non-interacting beam particles.

The forward-going particles are analysed in the magnetic spectrometer which consists of two dipole magnets, 48 planes of large drift chambers and three multicellular threshold Cherenkov counters for particle identification. Results are presented on the analysis of 331,000 kaon-induced triggers and 870,000 pion-induced triggers collected in November 1981 in a parasitic experiment of the NA11 charm search program.

The sensitivity of the experiment for incident kaons is (40.6±4.5) nb per nucleon per event, and for incident pions (16.2±2.0) nb per nucleon per event, assuming linear A dependence.

3. DATA ANALYSIS

Charged hadrons are reconstructed with an efficiency of 95% per track. The mass resolution has been measured to be on an average 9 MeV at the K^* mass, and checked with known particles such as the ρ, K^o_S, ϕ, and Λ [6]. Events are selected which have at least two oppositely charged particles, one being an identified kaon and the other a pion. The pulse-height information from the cells of the Cherenkov counters is used to distinguish π from K or p in the momentum range 4-14 GeV, and to separate unambiguously π, K and p from 14 to about 75 GeV. The identification efficiency as a function of momentum has been determined experimentally: the number of $\bar{K}^{*o}$ events produced in K^-Be interactions in the mass spectra are calculated once by assigning the kaon mass to one partner of a two particle combination, and once by using the Cherenkov identification, and the two results are compared. The inefficiency in the kaon identification, mainly due to overlapping particles in the Cherenkov cells, is on an average 20%.

Figure 2 shows the invariant $K^-\pi^+$ and $K^+\pi^-$ mass spectra for both types of incoming particles. The number of K^* events in each spectrum is obtained by fitting a p-wave Breit-Wigner superimposed on a polynomial times exponential background, and by correcting the result of the fit for the acceptance of the apparatus. The acceptance is calculated for an isotropic decay of the K^* into $K\pi$ and is shown in fig. 3 as a function of Feynman x (x_F). The isotropy of the decay has been verified experimentally by looking at the angular distribution of the kaon in the K^* rest frame for three different x_F regions. The p_T^2 dependence of the acceptance is flat in the range $0 < p_T^2 < 5$ GeV^2. The acceptance corrections include geometrical cuts, kaon-identification efficiency, track reconstruction and triggering efficiencies.

Owing to the threshold settings of the Cherenkov counters, pions can be wrongly identified as kaons, in particular at high momenta. Thus the $K\pi$ invariant mass distributions include reflections from $\pi\pi$ resonances coming from the combination of a pion misidentified as a kaon and another pion.

To account for the influence of those reflections in our invariant mass spectra, we proceed in the following way: first we form as a function of x_F the invariant mass spectra of each two unambiguously identified pion combinations produced in π^-Be interactions. The ρ resonance is predominant in all mass spectra so that we conclude that the reflections in the Kπ mass spectrum come from the ρ meson. We then assign the kaon mass to one pion of the combination and fit the resulting mass spectra with a Breit-Wigner function together with a polynomial times exponential background, the Breit-Wigner function being a good approximation to the shape of the reflection. The reflection has a peak at 960 MeV and a FWHM of 150 MeV. This procedure gives us the location of the ρ reflection. Finally we introduce these results as an additional Breit-Wigner term REFL in the invariant mass fits. The cross-section, as a function of the invariant mass, is now fitted in the range 0.65 to 1.65 GeV^2 as

$$\frac{d\sigma}{dM} = BG + \alpha PS \cdot BW + \beta PS \cdot REFL,$$

where

$BG = (a+bM+cM^2+dM^3)e^{fM}$.

PS = phase space factor

BW = relativistic p-wave Breit-Wigner

α,β,a-d,f : free parameters

The masses and widths of the K^* and of the ρ reflection were kept fixed in the individual fits. The contribution of the ρ reflection was found to be less than a few percent for $x_F < 0.6$, and about 25% in the x_F bin: $0.8 < x_F < 0.9$. For $x_F \geq 0.7$, it was sufficient to use a second-order polynomial for the background, and we had to add another Breit-Wigner term describing the $K^*(1430)$ resonance.

4. RESULTS

4.1 Differential Cross-Sections

We present results in the ranges $0 < x_F < 1.0$ and $0 < p_T^2 < 5$ GeV^2. They were obtained by fitting the invariant mass spectra in each x_F and p_T^2 bin as described in the section on data analysis. Figure 4 shows as an example the invariant $K^-\pi^+$ mass distribution for the K^--induced reaction together with the result of the fit in the range $0.5 < x_F < 0.6$.

4.1.1 Longitudinal momentum distributions

The $d\sigma/dx_F$ distribution and the invariant differential cross-section

$$f(x_F) = \frac{1}{\pi} \int \frac{E^*}{p^*_{max}} \frac{d^2\sigma}{dx_F dp_T^2} dp_T^2$$

where

E^* : K^* centre-of-mass energy

p^*_{max} : maximum centre-of-mass K^* longitudinal momentum

for $\bar{K}^{*o}$ and K^{*o} production induced by kaons are presented in table 1. The invariant x_F distributions are also shown in fig. 5. We have fitted the invariant cross-section $f(x_F)$ by the simple function $(1-x_F)^{n_2}$ suggested by the quark counting rules whose predictions are compared with data [5,6], and which have been recently linked to perturbative QCD by Gunion [5]. The $\bar{K}^{*o}$ data can be fitted in the fragmentation range $0.3 < x_F < 0.9$ with $n_2 = 0.46 \pm 0.10$, while for the K^{*o} the x_F range is $0.1 < x_F < 0.6$ and $n_2 = 2.70 \pm 0.45$.

The differential cross-sections $d\sigma/dx_F$ and $f(x_F)$ for $\bar{K}^{*o}$ and K^{*o} production induced by pions are presented in table 2. The data points for $f(x_F)$ are shown in fig. 6. Both distributions can be fitted in the x_F range $0.3 < x_F < 0.9$ by the function of form $(1-x_F)^{n_2}$, where $n_2 = 1.47 \pm 0.51$ for $\bar{K}^{*o}$ and $n_2 = 0.56 \pm 0.13$ for K^{*o}.

Table 3 summarizes the results of the fits to $f(x_F)$. The results of the fits to $d\sigma/dx_F$ are also shown to allow comparison with earlier experiments [3b]. Results of other experiments are presented together with the Gunion quark-counting-rules predictions [5].

In the fragmentation region $0.3 < x_F < 0.9$, the observed reactions are well represented by functions of the form $(1-x_F)^{n_2}$. The value of n_2 found for the reaction (a) is in agreement with other experiments at different energies [3c,3h,3e], but is systematically lower, as well as the n_2 value for reaction (d), than the quark-counting-rules predictions. One should take into account the fact that the data points for reaction (b) all lie below $x_F = 0.6$ when comparing the result for n_2 with the prediction. The value of n_2 found for reaction (c) lies below the prediction, but agrees with a result found at 32 GeV for proton-induced K^{*+} production [3i].

Figure 7 shows the x_F dependence of the following invariant cross-section ratios. In fig. 7a we display the ratios of the leading to the non-leading channel cross-section for the kaon- and pion-induced reactions. Note the rise of both ratios with growing x_F, and the spectacular growth of the kaon-induced cross-section ratio. This is probably related to the higher mass of the s quark and its harder structure function. Figure 7b shows the ratio of the leading channel cross-section induced by kaons to the leading channel cross-section induced by pions, and the ratio of the non-leading channel cross-section induced by kaons to the non-leading channel induced by pions, normalized to the respective inelastic cross-sections. The flattening of the ratio of the leading channel cross-sections in the region $0.3 < x_F < 0.9$ indicates that both the s quark and the d quark fragment in the same way. The cross-section ratio for the non-leading channels shows a slight decrease starting at $x_F = 0.4$. One needs more statistics in the $K^-Be \rightarrow K^{*o}X$ channel to make a statement about the respective fragmentation properties.

4.1.2 Tranverse momentum distributions

The $d\sigma/p_T^2$ distribution and

$$f(p_T^2) = \frac{1}{\pi} \int \frac{E^*}{p^*_{max}} \frac{d^2\sigma}{dx_F dp_T^2} dx_F$$

are presented in tables 4 and 5 and shown in figs. 8 and 9 for the kaon- and pion induced reactions. If one limits oneself to the range $0 < p_T^2 < 1$ GeV^2, all the distributions can be represented by a function of the form $A\, e^{-bp_T^2}$ with $\langle b \rangle = 2.45 \pm 0.18$. Table 6 summarizes the results of the fits and presents results from other experiments. Reactions (b) and (c) can be well fitted over the range $0 < p_T^2 < 5$ GeV^2, whereas reactions (a) and (d) cannot. For $p_T^2 > 1$ GeV^2, one observes a break in all the distributions to a flatter p_T^2 dependence, with a slope slightly less than 2 GeV^{-2}, and equal for the four reactions within the statistics available. These results, allowing for the fact that in other experiments fits are performed with non-invariant p_T^2 distributions, are in agreement with the results of refs.[3c,3i], but the values for b found in refs.[3a,3b,3f] are all higher.

4.2 Integrated Cross-Sections

Table 7 shows the observed number of K^* events in each channel and for each incident particle. The integrated cross-sections are obtained by fitting the invariant mass spectra taken over the range $0 < x_F < 1$. In table 8 we show the integrated cross-section ratios introduced earlier. Ratios (1) and (2) are ratios of invariant cross-sections of leading particle to non-leading particle channels for incident kaons and pions. One sees that the s quark is much more suppressed than the d quark. Another way of looking at this is to compare the invariant cross-section induced by kaons with that induced by pions [ratios (3) and (4)]. The ratio of the leading channels (3) is 4, whereas for the non-leading channels (4) it is close to 1.

4.3 A Dependence of K^--induced $\bar{K}^{*o}$ Inclusive Production

We compare now K^--induced $\bar{K}^{*o}$ production on beryllium with $\bar{K}^{*o}$ production on hydrogen investigated by Göttgens et al. [3f]. The two cross-sections are related by the formula:

$$\sigma(A) = \sigma(p)A^{\alpha}$$

Barton et al. [7] found that the α parameter was weakly decreasing with x_F in 100 GeV proton fragmentation into pions, kaons, protons and anti-protons on different nuclear targets.

Table 9 presents our results in different x_F bins, which we also show in fig. 10 together with a curve obtained by a fit to proton fragmentation data [7].

Our data points show the same decrease of α with x_F. One should, however, point out that the beryllium mass is still very close to the hydrogen mass, and that our results on the differential distributions are in good agreement with results of other experiments on proton targets.

5. CONCLUSIONS

We have measured inclusive $\bar{K}^{*o}$ and K^{*o} production on beryllium by negative kaons and pions at 175 GeV in the ranges $0<x_F<1.0$ and $p_T^2 \leq 5$ $(GeV)^2$. We have investigated production properties of leading and non-leading particle channels.

Both integrated and differential cross-sections demonstrate a leading particle effect, namely that $\bar{K}^{*o}$ in the kaon induced reaction and K^{*o} in the pion induced reaction are produced more strongly than K^{*o} and $\bar{K}^{*o}$, respectively. The effect is bigger in the kaon induced case, which might be related to the s quark mass.

The invariant cross-sections $f(x_F)$ for $x_F \geq 0.3$ of the kaon and pion induced reactions can be well described by a function of the form $(1-x)^n$, but the values found for n do not agree with those expected from quark counting rules, except for the non-leading K^-- induced reaction. However, in this case, we have data points only up to $x_F = 0.6$.

The function $e^{-bp_T^2}$ describes very well all p_T^2 distributions, with an average $\langle b \rangle = 2.45 \pm 0.18$, up to $p_T^2 = 1$ GeV^2. The distributions flatten out when $p_T^2 > 1$ GeV^2.

We investigated the A dependence of K^--induced inclusive K^{*o} production from hydrogen to beryllium using our data and those of Göttgens et al. [3f] taken on hydrogen. The parameter α shows the same x_F dependence as found by Barton et al. [7] in single-particle inclusive production.

Acknowledgements

We would like to acknowledge the contribution of the SPS crew to the success of the experiment. We wish to thank Dr. K. Fialkowski for very useful suggestions. We also wish to express our thanks for the many important contributions of the technical staff of the participating institutes. The members of the Cracow group would like to thank MPI, CERN and NIKHEF-H for their support and hospitality.

REFERENCES

[1] P.D.B. Collins and A.D. Martin, Rep. Prog. Phys. 45 (1982) 335.

[2] K. Fialkowski, W. Kittel, Rep. Prog. Phys. 46 (1983) 1283.

[3] a) C. Cochet et al., Nucl. Phys. B155 (1979) 333;
b) K. Böckmann et al., Nucl. Phys. B166 (1980) 284;
c) I.V. Ajinenko et al., Z. Phys. C 5 (1980) 177;
d) P.V. Chliapnikov et al., Z. Phys. C 12 (1982) 99;
e) E.A. de Wolf et al., Z. Phys. C 12 (1982) 105;
f) R. Göttgens et al., Z. Phys. C 12 (1982) 323;
h) M. Barth et al., Nucl. Phys. B223 (1983) 296;
i) E.A. Starchenko et al., Z. Phys. C 16 (1983) 181.

[4] W. Spierenburg, Ph.D. thesis, NIKHEF-H, Amsterdam 1983.

[5] J.F. Gunion, Phys. Lett. 88B (1979) 150.

[6] V. Bakken et al., Nuovo Cimento. 66A (1981) 71.
D. Denegri et al., Phys. Lett. 98B (1981) 127.

[7] D.S. Barton et al., Phys. Rev. D26 (1982) 1497.

Table 1 K^--induced differential cross-sections $d\sigma/dx_F$ and $f(x_F)$ for $\bar{K}^{*o}$ and K^{*o}.

	$\bar{K}^{*o}$		K^{*o}	
x_F range	$d\sigma/dx_F$ (mb)	$f(x_F)$ (mb)	$d\sigma/dx_F$ (mb)	$f(x_F)$ (mb)
0.0–0.1	1.88±0.19	0.111±0.009	0.85±0.16	0.051±0.008
0.1–0.2	2.24±0.14	0.179±0.009	0.84±0.10	0.067±0.007
0.2–0.3	1.97±0.11	0.220±0.011	0.47±0.06	0.049±0.006
0.3–0.4	1.75±0.10	0.244±0.013	0.24±0.04	0.036±0.006
0.4–0.5	1.43±0.13	0.244±0.021	0.15±0.04	0.023±0.007
0.5–0.6	1.16±0.12	0.211±0.023	0.06±0.03	0.009±0.005
0.6–0.7	1.10±0.12	0.205±0.037		
0.7–0.8	0.78±0.24	0.152±0.018		
0.8–0.9	0.75±0.13	0.132±0.029		
0.9–1.0	0.89±0.23	0.086±0.032		

Table 2 π^--induced differential cross-sections $d\sigma/dx_F$ and $f(x_F)$ for $\bar{K}^{*o}$ and K^{*o}.

	$\bar{K}^{*o}$		K^{*o}	
x_F range	$d\sigma/dx_F$ (mb)	$f(x_F)$ (mb)	$d\sigma/dx_F$ (mb)	$f(x_F)$ (mb)
0.0–0.1	1.55±0.12	0.055±0.005	0.72±0.14	0.061±0.005
0.1–0.2	0.98±0.08	0.050±0.004	1.49±0.09	0.076±0.004
0.2–0.3	0.62±0.05	0.044±0.004	0.88±0.05	0.065±0.004
0.3–0.4	0.27±0.03	0.028±0.004	0.56±0.04	0.056±0.004
0.4–0.5	0.19±0.03	0.025±0.004	0.42±0.04	0.054±0.006
0.5–0.6	0.10±0.03	0.014±0.004	0.31±0.04	0.044±0.006
0.6–0.7	0.06±0.03	0.008±0.005	0.24±0,04	0.042±0.007
0.7–0.8	0.04±0.03	0.010±0.006	0.15±0.02	0.030±0.005
0.8–0.9	0.03±0.02	0.008±0.005	0.14±0.03	0.029±0.007
0.9–1.0	0.03±0.03	0.010±0.007	0.06±0.03	0.021±0.009

Table 3 Results of fits to x_F distributions.
Values of the exponents n_1, n_2 coming from the fit of $d\sigma/dx_F = A(1-x_F)^{n_1}$ and the function $f(x_F) = B(1-x_F)^{n_2}$ to the data for different ranges of x_F, together with results from other experiments and quark-counting rules predictions.

Reaction	p_{lab} (GeV)	x_F range (GeV^2)	n_1	$P(x^2)$	n_2	$P(x^2)$	n predicted by Gunion rule [5]
a) $K^-Be \to \bar{K}^{*o}X$	175	0.1–0.9	0.77±0.09	0.54	–	–	
		0.3–0.9	0.66±0.12	0.50	0.46±0.10	0.90	1
b) $K^-Be \to K^{*o}X$	175	0.1–0.6	4.32±0.55	0.88	2.70±0.45	0.86	3
c) $\pi^-Be \to \bar{K}^{*o}X$	175	0.1–0.9	3.95±0.33	0.12	1.82±0.27	0.71	
		0.3–0.9	2.29±0.51	0.74	1.47±0.51	0.68	3
d) $\pi^-Be \to K^{*o}X$	175	0.1–0.9	–	–	0.69±0.10	0.75	
		0.3–0.9	1.23±0.14	0.33	0.56±0.13	0.89	1
$K^+p \to K^{*+}X$ [3e]	32	≥ 0.3	–	–	0.30±0.06	0.61	1
$K^+p \to K^{*o}X$ [3c]		≥ 0.2	–	–	0.11±0.04	–	1
$K^+p \to K^{*+}X$ [3h]	70	≥ 0.2	–	–	0.31±0.12	–	1
$K^+p \to K^{*o}X$ [3h]		≥ 0.4	–	–	0.16±0.06	–	1
$\pi^+p \to K^{*+}X$ [3b]	16	< 0	3.10±0.30	–	–	–	3
$pp \to K^{*+}X$ [3b]	24	all	3.10±0.30	–	–	–	3
$\bar{p}p \to K^{*+}X$ [3i]	32	all	–	–	1.64±0.38	–	3

Table 4 K^--induced differential cross-sections $d\sigma/dp_T^2$ and $f(p_T^2)$ for $\bar{K}^{*o}$ and K^{*o}.

	$\bar{K}^{*o}$		K^{*o}	
p_T^2 range $(GeV/c)^2$	$d\sigma/dp_T^2$ (mb)	$f(p_T^2)$ (mb)	$d\sigma/dp_T^2$ (mb)	$f(p_T^2)$ (mb)
0.0-0.1	2.28±0.34	0.662±0.060	1.70±0.20	0.104±0.029
0.1-0.2	4.94±0.25	0.447±0.047	1.44±0.17	0.081±0.026
0.2-0.4	3.25±0.15	0.294±0.027	0.94±0.09	0.055±0.015
0.4-0.6	2.07±0.11	0.202±0.022	0.54±0.07	0.026±0.010
0.6-0.8	1.32±0.09	0.149±0.021	0.29±0.05	0.019±0.008
0.8-1.0	0.65±0.07	0.070±0.015	0.21±0.04	0.016±0.007
1.0-1.5	0.35±0.03	0.040±0.006	0.07±0.02	0.006±0.003
1.5-2.0	0.15±0.02	0.018±0.004	0.014±0.013	0.001±0.002
2.0-3.0	0.06±0.01	0.007±0.002	0.013±0.006	0.001±0.001
3.0-5.0	0.012±0.003	0.002±0.001	0.003±0.002	0.0008±0.0008

Table 5 π^--induced differential cross-sections $d\sigma/dp_T^2$ and $f(p_T^2)$ for $\bar{K}^{*o}$ and K^{*o}.

	$\bar{K}^{*o}$		K^{*o}	
x_F^2 range $(GeV/c)^2$	$d\sigma/dp_T^2$ (mb)	$f(p_T^2)$ (mb)	$d\sigma/dp_T^2$ (mb)	$f(p_T^2)$ (mb)
0.0-0.1	1.83±0.14	0.106±0.019	2.83±0.16	0.185±0.023
0.1-0.2	1.49±0.10	0.082±0.017	2.11±0.12	0.134±0.019
0.2-0.4	1.06±0.06	0.060±0.010	1.33±0.07	0.096±0.011
0.4-0.6	0.55±0.05	0.030±0.007	0.84±0.05	0.061±0.008
0.6-0.8	0.32±0.04	0.023±0.006	0.50±0.04	0.039±0.007
0.8-1.0	0.20±0.03	0.015±0.005	0.25±0.03	0.022±0.006
1.0-1.5	0.08±0.01	0.006±0.002	0.16±0.02	0.016±0.003
1.5-2.0	0.03±0.01	0.003±0.002	0.06±0.01	0.006±0.002
2.0-3.0	0.017±0.004	0.0014±0.0007	0.024±0.004	0.003±0.001
3.0-5.0	0.004±0.03	0.0004±0.0004	0.005±0.001	0.0006±0.0003

Table 6 Results of fits to p_T^2 distributions.
Values of the exponent b coming from the fit of the function $f(p_T^2) = A\, e^{-bp_T^2}$ to the data in several p_T^2 ranges, together with the results from other experiments.

Reaction	p_{lab} (GeV)	p_T^2 range (GeV^2)	A (mb·GeV^{-2})	b (GeV^{-2})	P(χ^2)
a) $K^-Be \to \bar{K}^{*o}X$	175	0 -5.0	6.15±0.42	2.17±0.12	0.08
		0 -1.0	6.71±0.52	2.45±0.20	0.34
		1.0-5.0	0.85±0.30	1.91±0.21	0.57
b) $K^-Be \to K^{*o}X$	175	0 -5.0	1.11±0.24	2.43±0.42	0.97
		0 -1.0	1.14±0.27	2.53±0.69	0.95
		1.0-5.0	0.09±0.15	1.77±0.90	0.74
c) $\pi^-Be \to \bar{K}^{*o}X$	175	0 -5.0	1.09±0.15	2.19±0.24	0.80
		0 -1.0	1.17±0.17	2.39±0.37	0.92
		1.0-5.0	1.00±0.07	1.72±0.40	0.94
d) $\pi^-Be \to K^{*o}X$	175	0 -5.0	1.72±0.16	1.95±0.14	0.40
		0 -1.0	2.00±0.20	2.42±0.25	0.99
		1.0-5.0	0.33±0.13	1.92±0.22	0.96

Reaction	p_{lab} (GeV)	p_T^2 range (GeV^2)	C (mb·GeV^{-2})	d (GeV^{-2})	P(χ^2)
$K^+p \to K^{*+}X$ [3c]	32	0.2-2.2	7.22±0.98	2.56±0.19	0.46
$K^+p \to K^{*o}X$ [3c]		0.2-2.2	7.02±0.80	2.54±0.15	0.57
$K^-p \to \bar{K}^{*o}X$ [3a]		0 -1.5	11.1±0.90	3.30±0.20	-
$K^-p \to K^{*o}X$ [3a]		0 -1.5	14.5±2.70	3.40±0.20	-
$K^-p \to \bar{K}^{*o}X$ [3f]	110	0 -1.7	16.8±2.70	3.50±0.40	-
$\pi^+p \to K^{*+}X$ [3b]	16	0 -1.7	-	3.10±0.20	-
$\pi^+p \to K^{*-}X$ [3b]		0 -1.7	-	3.80±0.50	-
$pp \to K^{*+}X$ [3b]	12	0 -1.7	-	3.60±0.40	-
$pp \to K^{*+}X$ [3b]	24	0 -1.7	-	3.20±0.30	-
$pp \to K^{*-}X$ [3b]		0 -1.7	-	3.30±0.50	-
$\bar{p}p \to K^{*o}X$ [3i]	32	0 -1.4	-	2.43±0.40	-

Table 7 Observed number of events in each channel and integrated non-invariant cross-sections in the range $0 < x_F < 1$.

	Observed number of events	Cross-section in mb *)
$K^-Be \to \bar{K}^{*o}X$	17 400±481	1.59±0.04±0.19
$K^-Be \to K^{*o}X$	4047±635	0.27±0.02±0.05
$\pi^-Be \to \bar{K}^{*o}X$	13 980±635	0.38±0.02±0.06
$\pi^-Be \to K^{*o}X$	21 120±716	0.61±0.02±0.09

*) The first error is statistical and the second systematic.

Table 8 Ratios of invariant cross-sections.
a) and b) Ratios of leading channel to non-leading channel cross-sections in K^--induced and π^--induced reactions.
c) The ratio of the leading channel cross-section for incident kaons to the leading channel cross-section for incident pions, normalized to the respective inelastic cross-sections.
d) The ratio of the non-leading channel cross-section for incident kaons to the non-leading channel cross section for incident pions, normalized to the respective inelastic cross-sections.

$$\frac{\sigma(K^- \to \bar{K}^{*o})}{\sigma(K^- \to K^{*o})} = 7.45\pm0.51 \qquad (1)$$

$$\frac{\sigma(\pi^- \to K^{*o})}{\sigma(\pi^- \to \bar{K}^{*o})} = 1.78\pm0.10 \qquad (2)$$

$$\frac{\sigma_{inel(\pi^-p)}}{\sigma_{inel(K^-p)}} \times \frac{\sigma(K^- \to \bar{K}^{*o})}{\sigma(\pi^- \to K^{*o})} = 3.99\pm0.17 \qquad (3)$$

$$\frac{\sigma_{inel(\pi^-p)}}{\sigma_{inel(K^-p)}} \times \frac{\sigma(K^- \to K^{*o})}{\sigma(\pi^- \to \bar{K}^{*o})} = 1.38\pm0.13 \qquad (4)$$

Table 9 x_F dependence of the α parameter used in the A-dependence parametrization of the cross-section for K^--induced $\bar{K}^{*o}$ inclusive production: $\sigma(Be) = \sigma(p)\, A^{\alpha}$. Errors are statistical only.

x_F range	α
0.0–0.2	0.66±0.23
0.2–0.4	0.68±0.18
0.4–0.6	0.53±0.15
0.6–0.8	0.40±0.20
0.8–1.0	0.45±0.25

Figure captions

Fig. 1 : ACCMOR forward spectrometer (top view).
MNP33,BBC : Large aperture spectrometer magnets.
DC2,DC3A-C : Drift chambers.
C1-3 : Multicell threshold Cherenkov counters.
MA,MB : Scintillator hodoscopes (not used in this experiment).
D2 : Small scintillation counter to reject non-interacting beam particles.

Fig. 2 : Invariant $K\pi$ mass spectra for the kaon and pion induced reactions.

Fig. 3 : Acceptance as a function of x_F of the $K\pi$ system.

Fig. 4 : Invariant $K^-\pi^+$ mass spectrum in the range $0.5<x_F<0.6$ for the kaon induced reaction.

Fig. 5 : The invariant differential cross-section $f(x_F)$ for K^--induced $\bar{K}^{*o}$ and K^{*o} inclusive production. The open dots show the $\bar{K}^{*o}$ and the black dots show the K^{*o} data. Errors are statistical only. The lines show the functions of the form $A(1-x)^n$ in the range $0.3 < x_F < 0.9$ as explained in the text.

Fig. 6 : The invariant differential cross-section $f(x_F)$ for π^--induced $\bar{K}^{*o}$ and K^{*o} inclusive production. The open dots show the $\bar{K}^{*o}$ and the black dots show the K^{*o} data. Errors are statistical only. The lines show the functions of the form $A(1-x)^n$ in the range $0.3 < x_F < 0.9$ as explained in the text.

Fig. 7 : Ratios of invariant cross-sections as a function of x_F.
a) Ratio of leading to non-leading channel cross-sections for the kaon-induced reactions (black dots) and pion-induced reactions (open dots)
b) Ratio of the leading channel cross-section induced by kaons to the leading channel cross-section induced by pions (black dots), and ratio of the non-leading channel cross-section induced by kaons to the non-leading channel cross-section induced by pions (open dots).

Fig. 8 : The invariant differential cross-section $f(p_T^2)$ for K^--induced $\bar{K}^{*o}$ and K^{*o} inclusive production. The line represents a function of the form $Be^{-bp_T^2}$ for $p_T^2 < 1$ GeV^2 as explained in the text.

Fig. 9 : The invariant differential cross-section $f(p_T^2)$ for π^--induced $\bar{K}^{*o}$ and K^{*o} inclusive production. The line represents a function of the form $Be^{-bp_T^2}$ for $p_T^2 < 1$ GeV^2 as explained in the text.

Fig. 10 : The x_F dependence of α used to parametrize the A dependence of the K^--induced $\bar{K}^{*0}$ inclusive production. The blacks dots are our data, whereas the curve is a result of a fit to proton fragmentation data, as explained in the text.

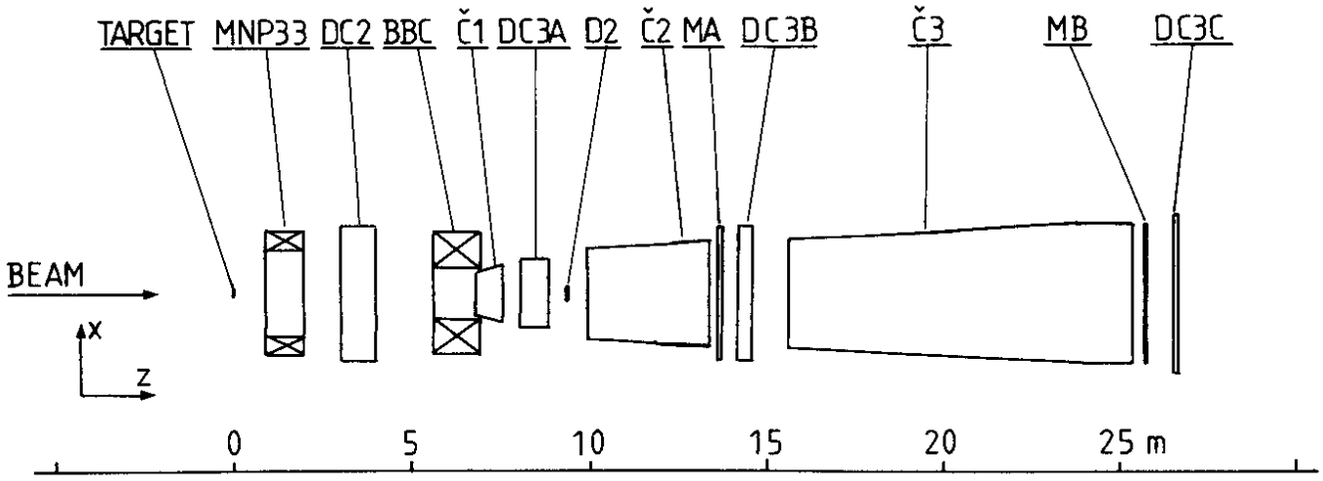
TARGET
MNP33
DC2
BBC
Č1
DC3A
D2
Č2
MA
DC3B
Č3
MB
DC3C
BEAM
x
z
0
5
10
15
20
25 m

Fig. 1

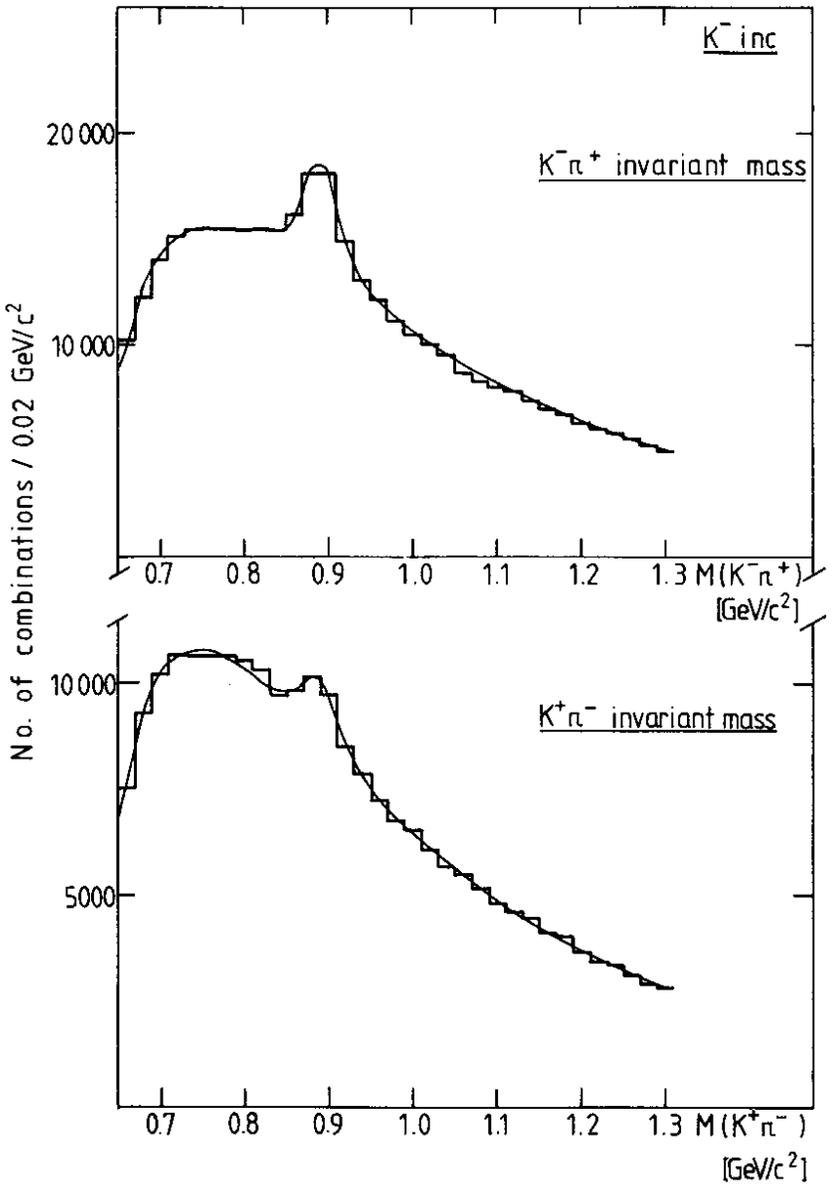
K⁻ inc
K⁻π⁺ invariant mass
20 000
10 000
No. of combinations / 0.02 GeV/c²
0.7 0.8 0.9 1.0 1.1 1.2 1.3 M(K⁻π⁺)
[GeV/c²]
K⁺π⁻ invariant mass
10 000
5000
0.7 0.8 0.9 1.0 1.1 1.2 1.3 M(K⁺π⁻)
[GeV/c²]

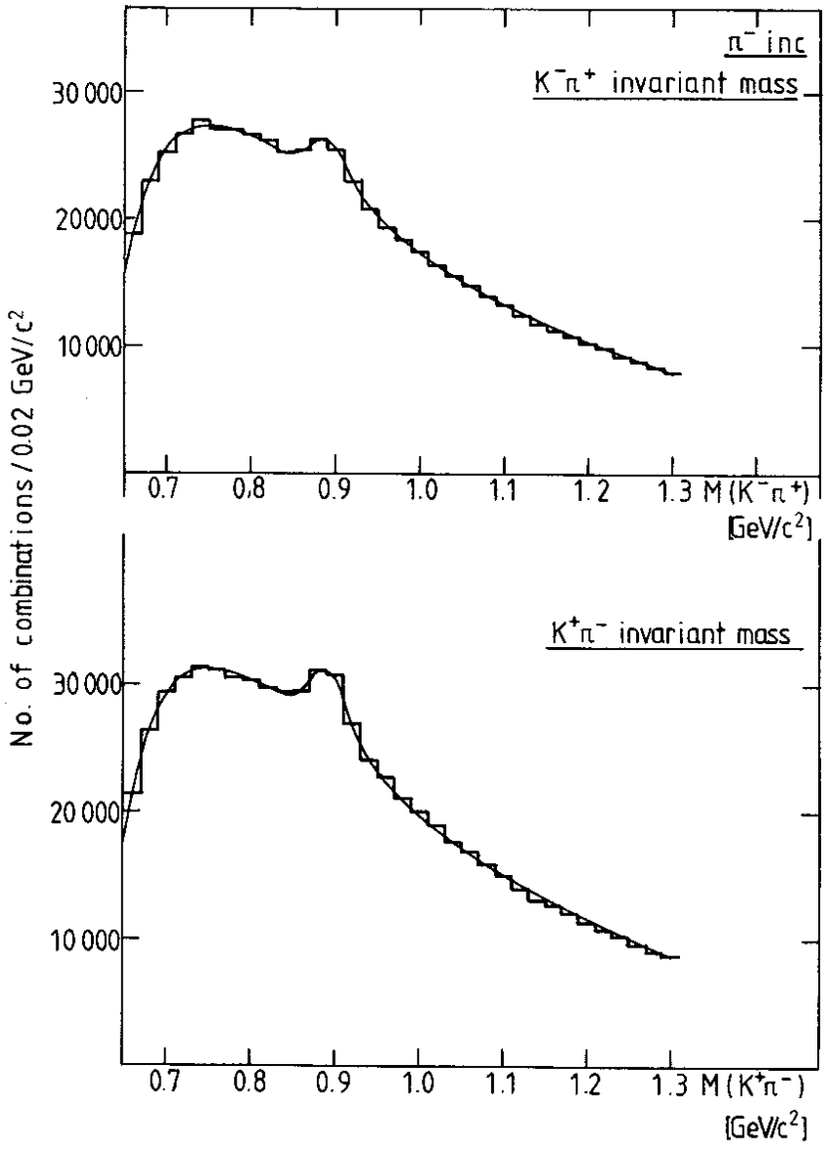
π⁻ inc
K⁻π⁺ invariant mass
30 000
20000
10 000
No. of combinations / 0.02 GeV/c²
0.7 0.8 0.9 1.0 1.1 1.2 1.3 M(K⁻π⁺)
[GeV/c²]
K⁺π⁻ invariant mass
30 000
20 000
10 000
0.7 0.8 0.9 1.0 1.1 1.2 1.3 M(K⁺π⁻)
[GeV/c²]

Fig. 2

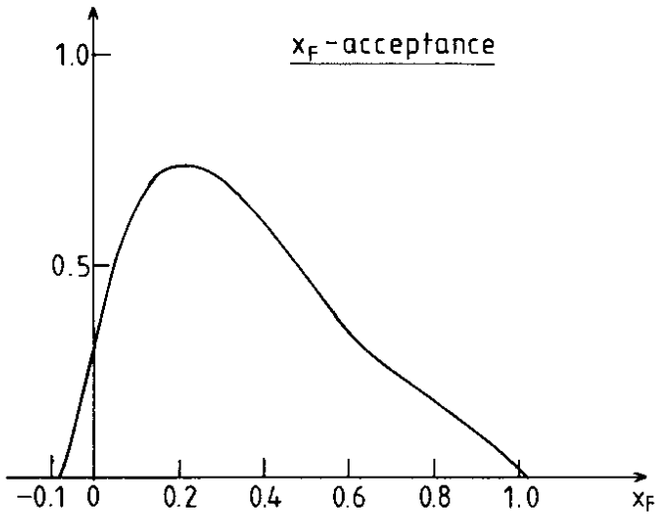
x_F - acceptance
1.0
0.5
−0.1
0
0.2
0.4
0.6
0.8
1.0
x_F

Fig. 3

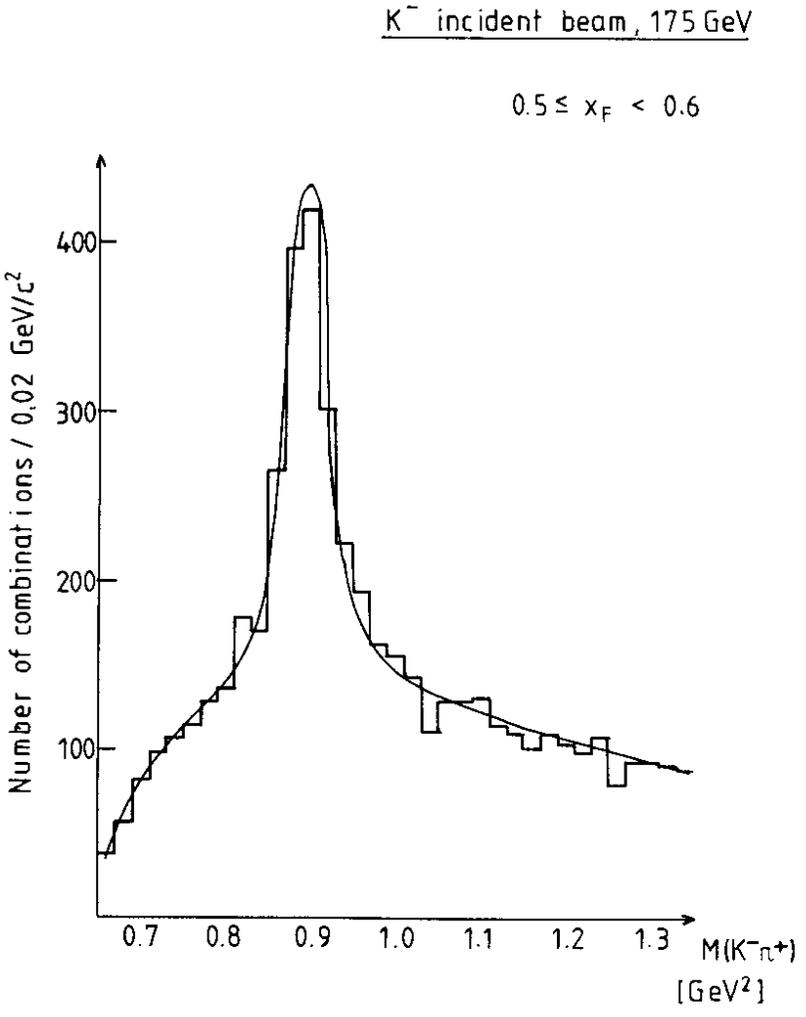
K^- incident beam, 175 GeV
$0.5 \leq x_F < 0.6$
Number of combinations / 0,02 GeV/c²
400
300
200
100
0.7
0.8
0.9
1.0
1.1
1.2
1.3
$M(K^-\pi^+)$
[GeV²]

Fig. 4

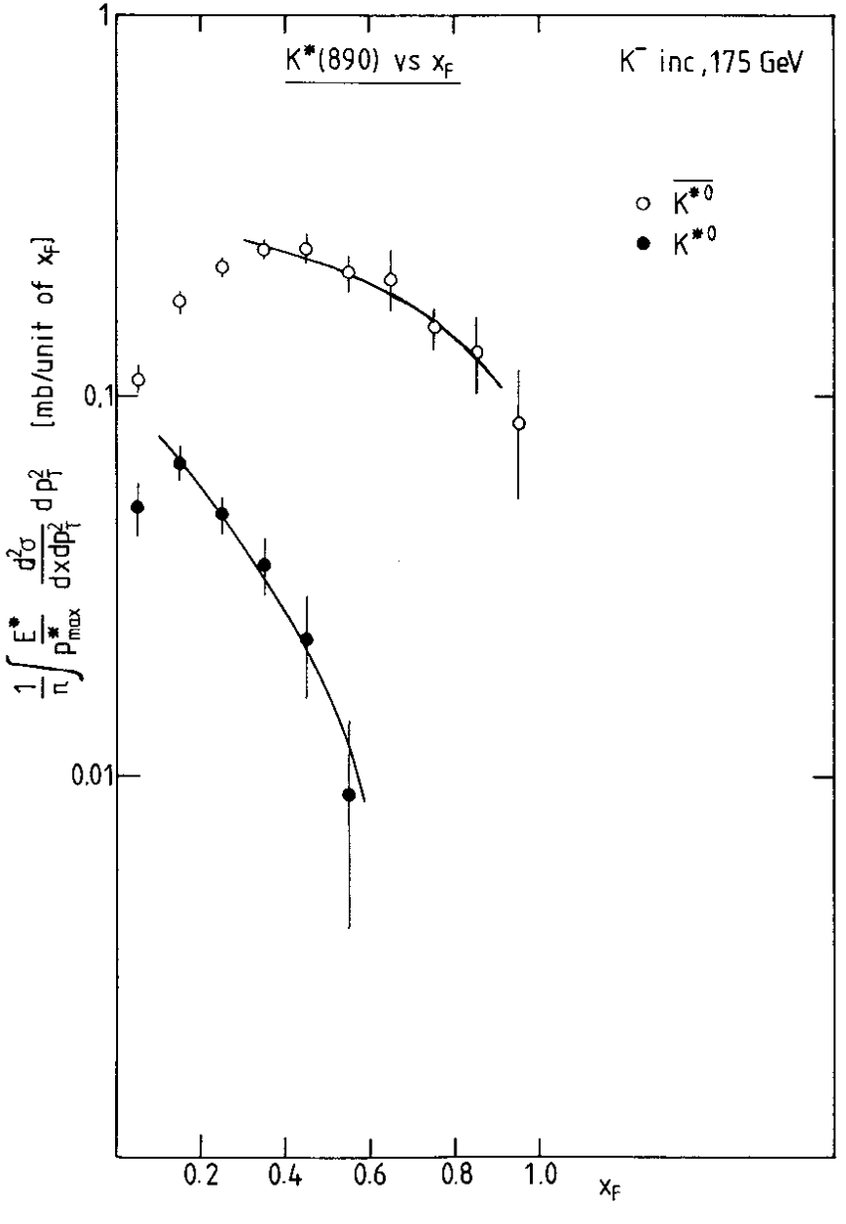
K*(890) vs x_F
K^- inc, 175 GeV
$\overline{K^{*0}}$
K^{*0}
$\frac{1}{\pi}\int\frac{E^*}{p^*_{max}}\frac{d^2\sigma}{dx\,dp_T^2}\,dp_T^2$ [mb/unit of x_F]
1
0.1
0.01
0.2
0.4
0.6
0.8
1.0
x_F

Fig. 5

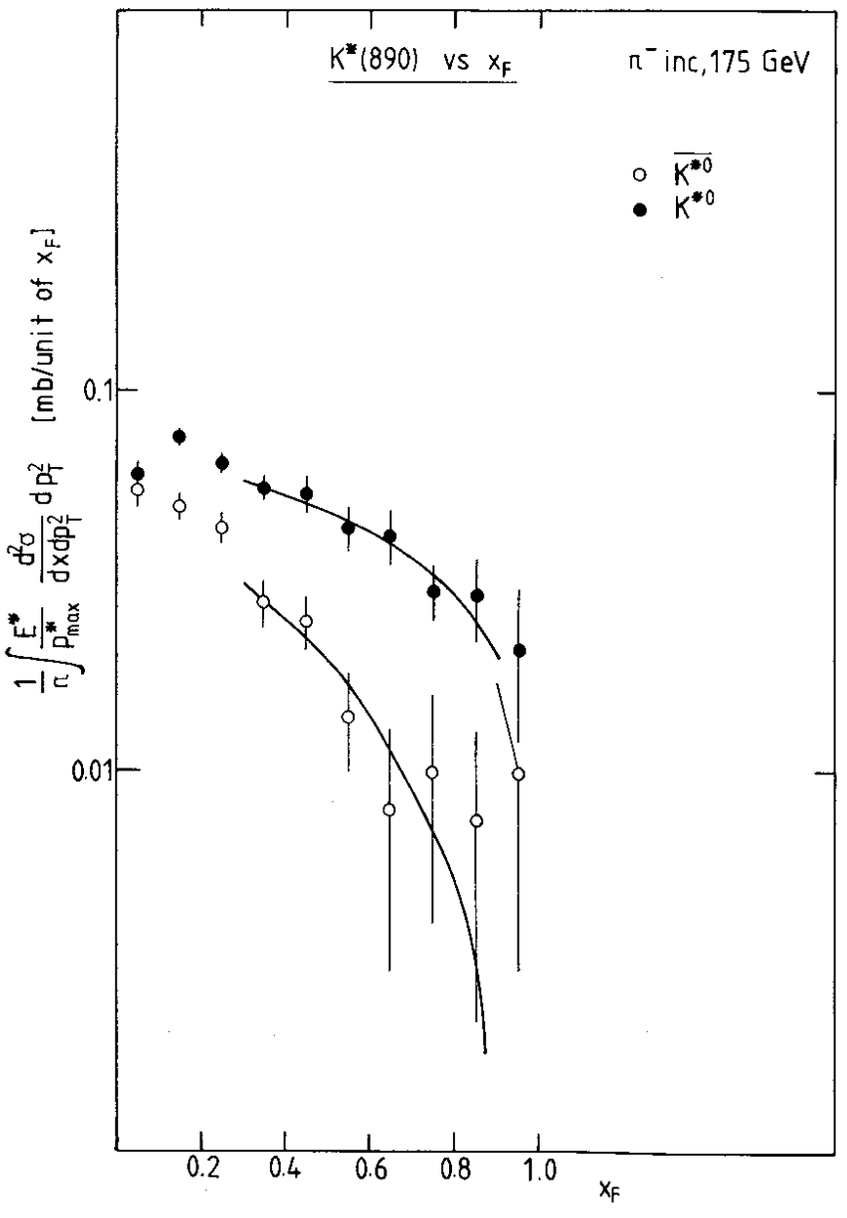
K*(890) vs x_F
π^- inc, 175 GeV
$\overline{K^{*0}}$
K^{*0}
$\frac{1}{\pi}\int\frac{E^*}{p^*_{max}}\frac{d^2\sigma}{dx\,dp_T^2}\,dp_T^2$ [mb/unit of x_F]
0.1
0.01
0.2
0.4
0.6
0.8
1.0
x_F

Fig. 6

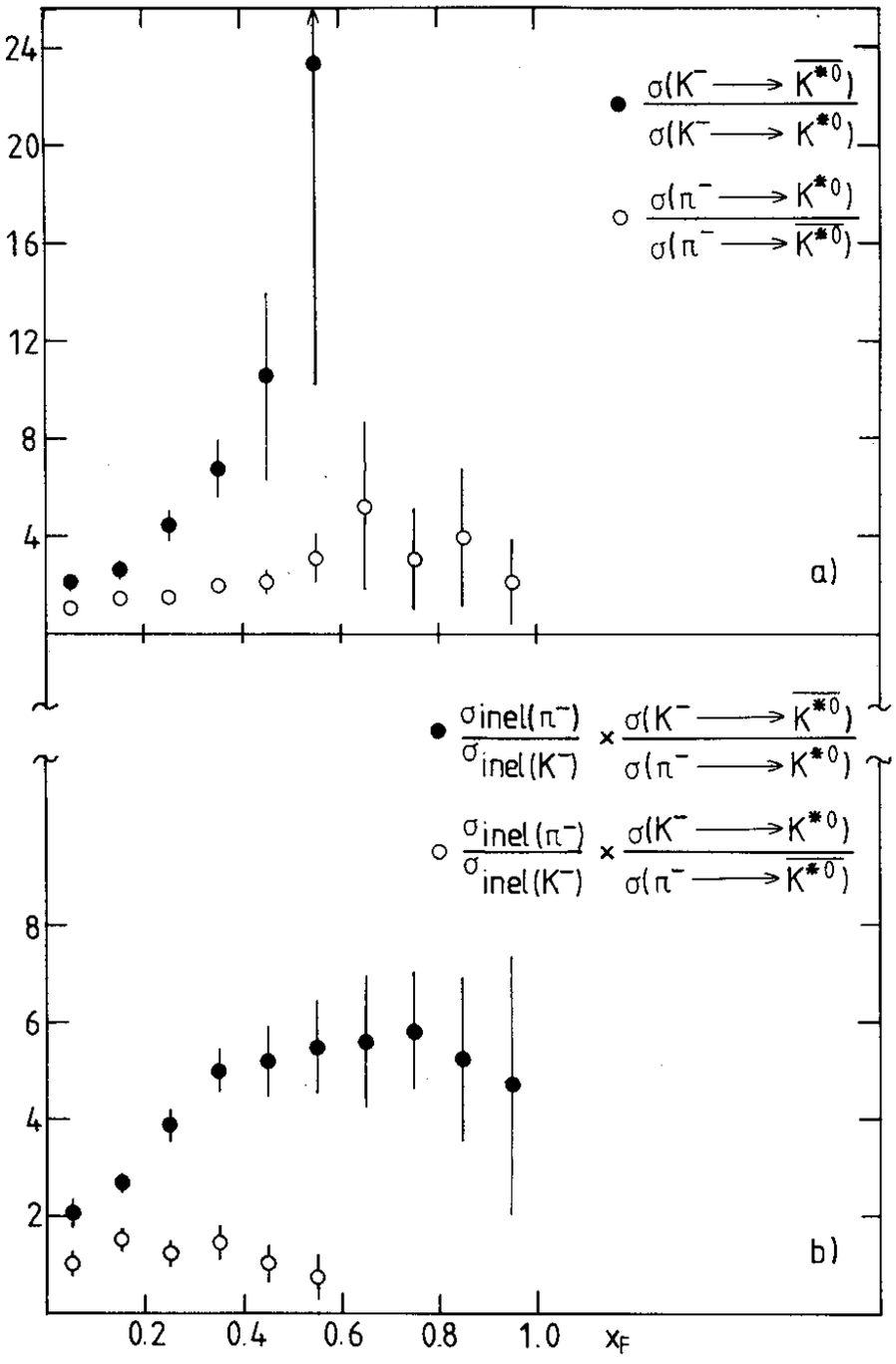

Fig. 7

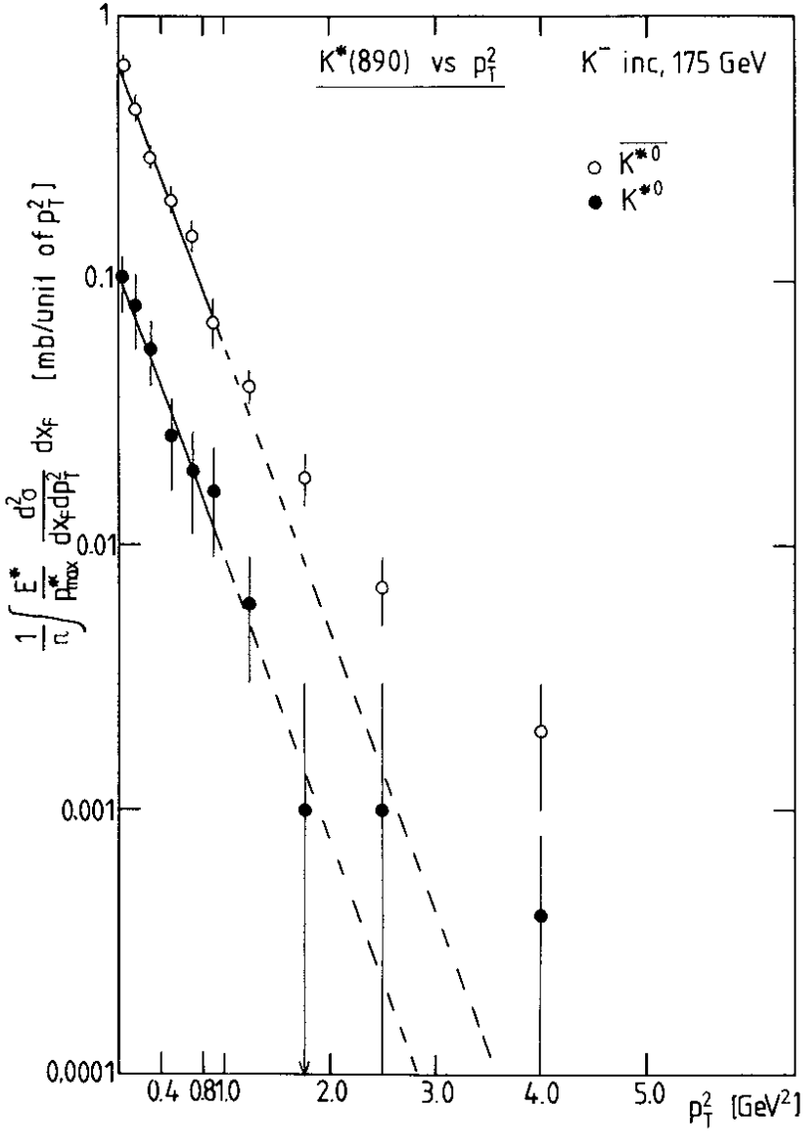
K*(890) vs p_T^2
K⁻ inc, 175 GeV
$\overline{K^{*0}}$
K^{*0}
$\frac{1}{\pi}\int \frac{E^*}{p^*_{max}} \frac{d^2\sigma}{dx_F dp_T^2} dx_F$ [mb/unit of p_T^2]
1
0.1
0.01
0.001
0.0001
0.4
0.8
1.0
2.0
3.0
4.0
5.0
p_T^2 [GeV^2]

Fig. 8

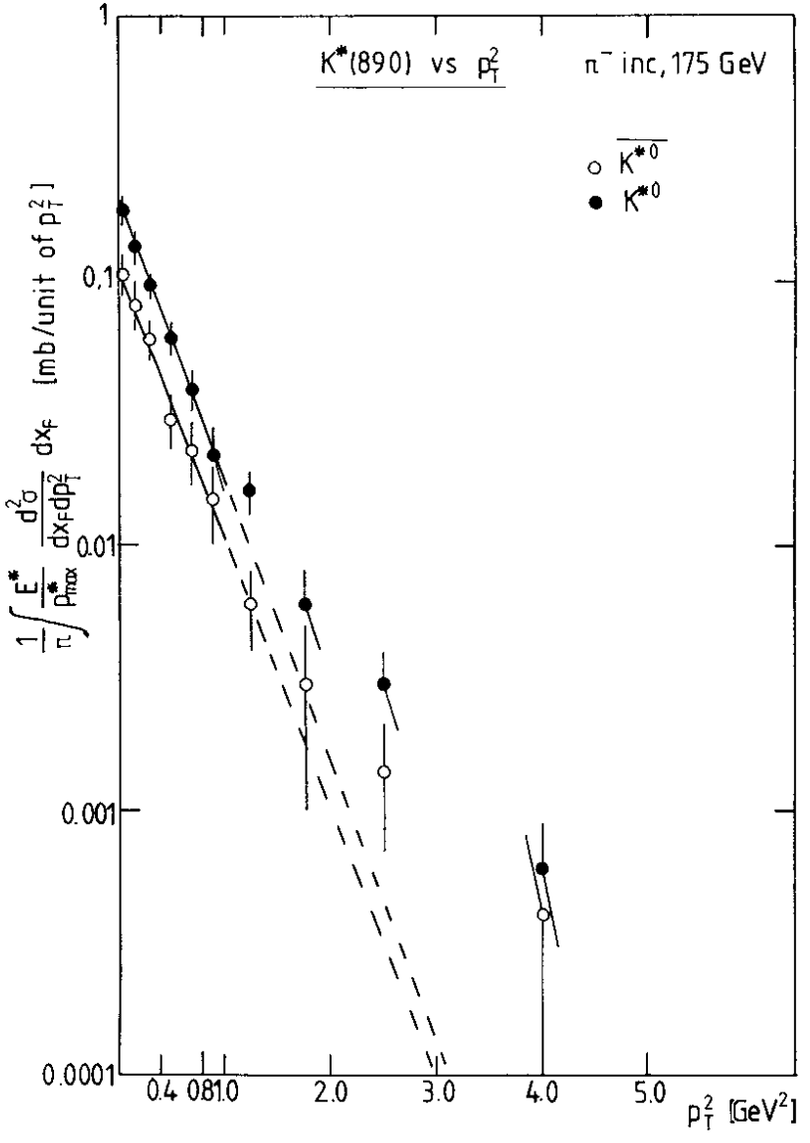
K*(890) vs p_T^2
π⁻ inc, 175 GeV
$\overline{K^{*0}}$
K^{*0}
$\frac{1}{\pi}\int \frac{E^*}{p^*_{max}} \frac{d^2\sigma}{dx_F dp_T^2} dx_F$ [mb/unit of p_T^2]
1
0.1
0.01
0.001
0.0001
0.4
0.8
1.0
2.0
3.0
4.0
5.0
p_T^2 [GeV^2]

Fig. 9

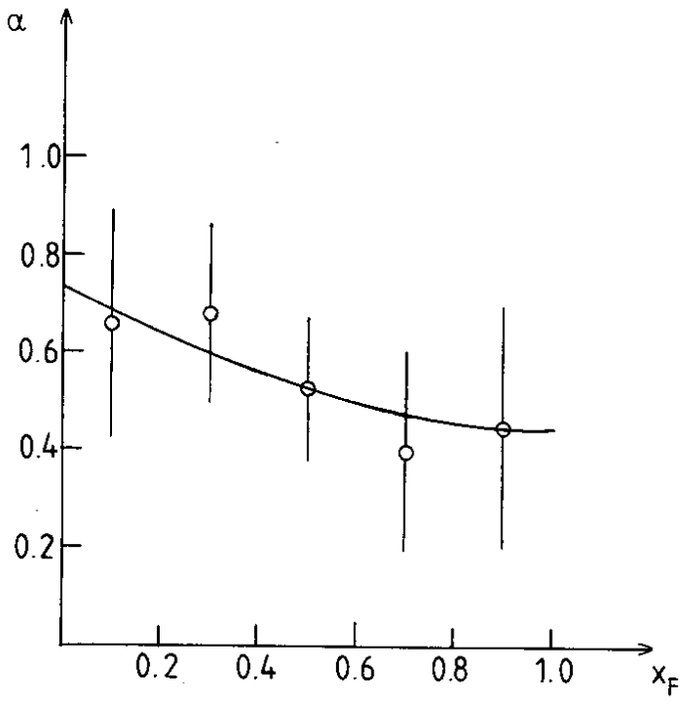

Fig. 10